PCCP

Accepted Manuscript

ROYAL SOCIETY OF CHEMISTRY

www.rsc.org/pccp

Journal Name

ARTICLE

The spectral relaxation dynamics and the molecular crowding effect of the silver nanoclusters synthesized in the polymer scaffold

Received 00th January 20xx,
Accepted 00th January 20xx

DOI: 10.1039/x0xx00000x

www.rsc.org/

Kai-Hung Wang,[a] and Chih-Wei Chang[a,*]

We have performed comprehensive study on the spectral relaxation dynamics of the silver nanoclusters (AgNCs) synthesized in the poly(methacrylic acid) (PMAA). In different polymer conformations and solvents, the spectral relaxation dynamics of the PMAA-AgNCs can be globally fitted by a bi-exponential decay, the short component is about 0.2~0.3 ns, whereas the long component is in the range between 1~3 ns. The spectral relaxation is associated with the energy transfer dynamics and the excitation of multiple emissive AgNCs. In this study, we have demonstrated the feasibility of using AgNCs as the fluorescence probe for fluorescence anisotropy studies. Meanwhile, the molecular crowding effects of the PMAA-AgNCs were addressed using the Triton X-100 reverse micelles. The results indicate that the fluorescence quantum yield of the AgNCs will be significantly increased in the crowded condition, which is beneficial for their usage in the intracellular image studies.

Introduction

In the past decade, the silver nanoclusters (AgNCs) have received considerable attentions due to their unique optical properties and potential applications in analytical chemistry, nano-electronics and biological studies.[1-16] The AgNCs are typically composed of 2-30 silver atoms and their size are <0.5 nm.[17] The limited number of silver atoms in AgNCs leads to the discrete energy level;[18, 19] and provides the missing link between single atom and plasmonic nanoparticles.[20] In order to avoid the aggregation, the AgNCs need to be synthesized in proper stabilizing scaffolds,[2] such as: dendrimers,[14] polymers,[7, 12, 21-23] polypeptides[24] and oligonucleotides.[5, 8, 10, 11, 13, 16, 25-29] By turning-on[30, 31] or turning-off[4] the fluorescence of the AgNCs, the AgNCs have been utilized as the molecular sensors for detecting protein,[32] oligonucleotides,[4, 6] metal ions[21, 30] and small molecules.[31] For the AgNCs synthesized in the DNA template, the silver salt is mixed with DNA and reduced by the $NaBH_4$. Junhua Yu et al. have demonstrated that the AgNCs can be synthesized in the polymer scaffold through the photo-reduction method and transferred to the DNA.[33] This strategy can avoid interference from the reducing agent; hence, it indicates many potential applications in biological studies. For the AgNCs synthesized in polymer scaffold, the absorption and emission spectra of the AgNCs show clear solvatochromic shifts,[34] which implies that the AgNCs might be a good fluorescence probe for studying the polarity of environment.

In previous studies, we have utilized the AgNCs as the fluorescence probe for studying the conformation changes of the human telomeric DNA.[35] To further address the fluorescence properties of the AgNCs in different templates, we have employed the poly(methacrylic acid) (PMAA) as the template for the AgNCs. The PMAA is ideal for studying the optical properties of the AgNCs in different template conformations, as it exhibits remarkable pH-induced conformation transition, and the conformation dynamics have been investigated in previous studies.[36, 37] Although the AgNCs have many potential applications in intracellular bio-image studies, most fluorescence studies regarding the AgNCs are performed in dilute solutions. In order to mimic the highly viscous[38] and crowded[39] conditions in the intracellular environment, we have employed the reverse micelles (RMs) and the PEG 400 to study the molecular crowding effects of the PMAA-AgNCs.[40] The highly structured and heterogeneous water pool inside the RMs closely resembles the biological interfacial water, and it has been utilized as the cell like container for the studies of encapsulated proteins[41] and DNAs.[42] Our findings suggest that the PMAA-AgNCs represent much higher fluorescence quantum yields in the molecular crowding condition created by the Triton X-100 RMs and 40 %

[a] Department of Chemistry, National Changhua University of Education, Changhua 50058, Taiwan

Electronic Supplementary Information (ESI) available: Figure S_1:The power and the emission spectra for the LED Lamp; Figure S_2~S_6:the fluorescence decays and the spectral relaxation dynamics of the PMAA-AgNCs in the glycerol, in the PVA film, solid powder, in the acetate buffer (λ_{ex}=445 nm) and in the MES buffer (λ_{ex}=445 nm); Figure S_7: The fluorescence anisotropy decay dynamics of the PMAA-AgNCs solid powder and in the PVA film; Figure S_8: The fluorescence intensity of the PMAA-AgNCs in three different reverse micelles; Figure S_9 and figure S_{10}: the fluorescence decays and the spectral relaxation dynamics of the PMAA-AgNCs in the 40% PEG400 solution and Triton X-100 reverse micelles; Table S_1: The fitting parameters of the spectral relaxation dynamics of the PMAA-AgNCs
See DOI: 10.1039/x0xx00000x

PEG 400 solution, and these findings are important for the applications of the AgNCs in the intracellular environment.

Experimental Section

Materials and sample preparation

The PMAA sodium salt solution (weight percentage=30%, averaged molecular weight=9500), $AgNO_3$ (>99%), MES (>99%), NaOH (>98%), glycerol(>99%), 1-hexanol (99%), polyvinyl alcohol (PVA, >99%), sodium bis(2-ethylhexyl) sulfosuccinate (AOT, 99%), cetrimonium bromide (CTAB, >99%) ,Triton X-100 (for electrolyte), PEG 400 (BioUltra) were purchased from Sigma Aldrich. The acetic acid (99.7%) was purchased from Macron. The HNO_3 solution (70%) was purchased from J. T. Baker. All chemicals were used as received. The deionized water (resistivity>18.2 MΩ-cm at 25°C) was obtained from the Barnstead™ EasyPure™ II water purification system (Thermo Scientific™) and used in all experiments. For the synthesis of PMAA-AgNCs, the pH of the PMAA sodium salt solution (concentration=0.36 g/ mL) was adjusted to 4.5 by adding HNO_3 solution[9] and then mixing with the 0.1 M $AgNO_3$ solution (volume ratio =1:1). The mixed sample was shining with the LED lamps for 40 hours (the spectra and the power of the LED lamps are indicated in the figure S_1). The prepared PMAA-AgNCs were stored in the dark and diluted to desired concentration before used. The solid powder of the PMAA-AgNCs was prepared by adding 83 % (volume percentage) of acetone into the stock solution and then collecting the precipitates in the bottom. The PVA film was prepared by mixing the PMAA-AgNCs with 15 % (weight percentage) PVA solutions and then paste-coating on glass plate.

Preparation of PMAA-AgNCs encapsulated reverse micelles

The details for preparing AOT and CTAB RMs has been described elsewhere.[42] For the AOT and CTAB RMs, the water content ($\omega = \frac{[\text{Water}]}{[\text{Surfactant}]}$) was controlled at 20. To prepare the Triton X-100 RMs, 0.32 mL 1-hexanol was mixed with 0.514 g Triton X-100 and 2.05 mL cyclohexane. The mixture was sonicated for 10 minutes. The solution was mixed with 80 μL of PMAA-AgNCs stock solution and then sonicated again until the solution become transparent.

Measurement of the size and spectroscopic properties

The hydrodynamic radius of the PMAA was measured by dynamic light scattering spectrophotometer (Horiba, SZ-100). A 10×3 mm quartz cuvette was used for measuring the absorption and emission spectra of the PMAA-AgNCs. The steady state UV-Vis absorption spectra were obtained using a Cary 100 spectrophotometer. The emission and excitation spectra were recorded by the Cary Eclipse fluorescence spectrophotometer. The fluorescence quantum yield of samples was estimated by using rhodamine 6G ethanol solution as the reference. The time-resolved fluorescence spectra were measured by the time-correlated photon counting spectrometer and the details have been reported previously.[35] The 510 nm light source was provided by a subnanosecond pulsed LED (PLS 500, Picoquant) in combination with a 510 nm band pass filter (FB510-10, Thorlabs) and a film polarizer. The polarization of the emission light was selected by the other film polarizer. For the solid samples, an additional long pass filter (FGL550, Thorlabs) was placed before the monochromator to avoid interference from the scattering light. The 445 nm excitation light source was provided by a vertical polarized picosecond-pulsed diode laser (LDH-440, Picoquant). For the fluorescence lifetime measurement, the polarization of the excitation light was set at the vertical position (relative to optical table) and the angle of the emission polarizer was set at 54.7° relative to the excitation light.

Results and Discussion

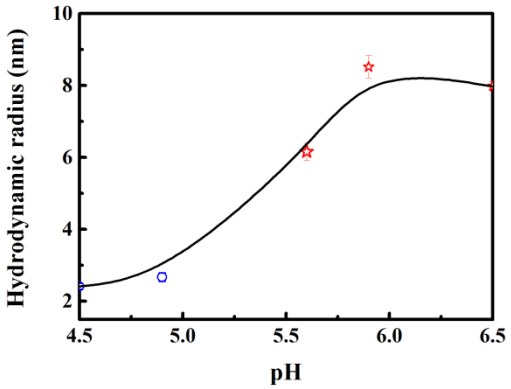

Figure 1: The hydrodynamic radius of the PMAA in different pH solutions. The blue circle and the red star indicate that the PMAA is dissolved in the acetate and MES buffers (concentration=20 mM), respectively

Figure 1 shows the hydrodynamic radius of the PMAA in different pH solutions. The results demonstrate that the PMAA undergoes conformational transition between pH=5 to pH=6. Below the transition point, the PMAA forms supercoil structure and the averaged hydrodynamics radius (r_H) of the PMAA was estimated to be ~2.4 nm. Above the transition point, the supercoil structure expends into water-swollen structure due to the repulsive interaction between the carboxylic group,[36] hence the hydrodynamics radius increases to about 8 nm. The conformational change also affects the spectroscopic properties of the AgNCs. Figure 2 demonstrates the fluorescence contour maps of the PMAA-AgNCs in the supercoil (in the acetate buffer, pH=4.5) and the water swollen (in the MES buffer, pH=6.5) conformations. In the acetate buffer, the emission peak of the PMAA-AgNCs is located at $\lambda_{excitation}/\lambda_{emission}$=490 nm/580 nm, and the fluorescence quantum yield is estimated to be 1.14 %. In the MES buffer, the fluorescence quantum yield of the AgNCs is drastically decreased to 0.09 % and the emission peak is red-shifted to $\lambda_{excitation}/\lambda_{emission}$=505 nm/610 nm. In the acetate and MES buffers, the emission spectra of the PMAA-AgNCs can be globally fitted by two emission bands. As excitation wavelength increases from 450 nm to 640 nm, the emission peak of the major emission band gradually shift toward longer wavelength, while the minor emission band is fixed at ~705 nm. In the figure 2c, we have summarized the emission peaks of the major emission band at different excitation wavelengths.

The previous studies suggested that the fluorescence of the AgNCs is due to the ligand-to-metal-metal charge transfer from the Ag(I)-carboxylate complex to the AgNCs.[43, 44] Therefore, the excitation dependent fluorescence is associated with the selective excitation of the AgNCs that exhibit different interaction energy with the environment.[44] To further address the excited state dynamics of the PMAA-AgNCs, we have performed complete time-resolved fluorescence measurement for the PMAA-AgNCs in the acetate and MES buffers (λ_{ex}=510 nm). The results are summarized in the Figure 3a and Figure 4a, respectively. As depicted, the fluorescence decays of the PMAA-AgNCs gradually slows-down toward longer emission wavelengths. This finding implies that the PMAA-AgNCs exhibits time-dependent spectral shifts in nanosecond time scale. To address this point, we have reconstructed the time-resolved emission spectra (TRES, Figure 3a and 4a, inset).[45] The TRES are fitted by log-normal equation and the spectral integral of the TRES at various delay time are calculated from the fitting parameters to represent the population decay dynamics of the PMAA-AgNCs (Figure 3b and 4b).[45] The peak positions at various delay time, ν(t), can be used to describe the spectral relaxation dynamics:

$$\nu(t) = \nu(\infty) + [\nu(0) - \nu(\infty)] \times (a_1 e^{-t/\tau_1} + a_2 e^{-t/\tau_2}) \quad (1)$$

The ν(0) and ν(∞) indicate the peak positions (in cm^{-1}) at t(0) and t(∞), respectively. The equation (1) can be further rearranged and the spectral response function C(t) can be defined by equation (2):

$$C(t) = \frac{\upsilon(t) - \upsilon(\infty)}{\upsilon(0) - \upsilon(\infty)} = a_1 e^{-t/\tau_1} + a_2 e^{-t/\tau_2} \quad (2)$$

where the fitting parameters are summarized in the Table S_1. Although the PMAA-AgNCs exhibit similar C(t) in the acetate ($\tau_{average}$=1.2 ns)and MES buffers($\tau_{average}$=1.4 ns), the relaxation energy ($\Delta\nu = \nu(0) - \nu(\infty)$) of the PMAA-AgNCs in the acetate buffer (604 cm^{-1}) is significantly larger than that in the MES buffer (319 cm^{-1}). To verify the origin of the spectral relaxation dynamics that we observed, we have measured the spectral relaxation dynamics of the PMAA-AgNCs in various environments, and the fitting parameters are also summarized in the Table S_1. In the glycerol solution (figure S_2, $\tau_{average}$=1.9 ns), the C(t) of the PMAA-AgNCs closely resembles that in the buffer solution. In the PVA film (figure S_3, $\tau_{average}$=1.4 ns) and solid powder (figure S_4, $\tau_{average}$=0.8 ns), the PMAA-AgNCs also represent similar C(t) but with much larger relaxation energy($\Delta\nu$=2260 cm^{-1} in the PVA film and 2416 cm^{-1} in the solid powder). The increase of relaxation energy in the solid matrix

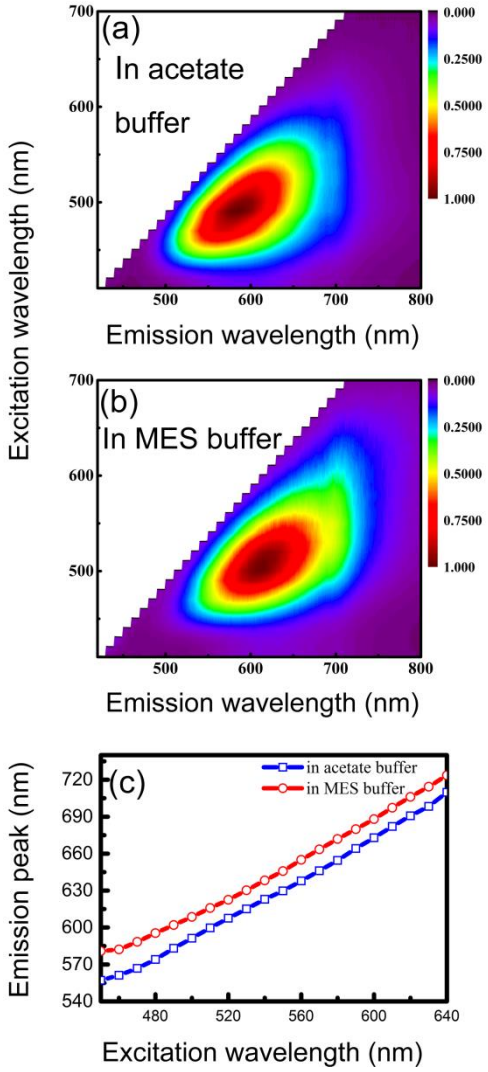

Figure 2: The fluorescence contour maps of the PMAA-AgNCs in (a) acetate and (b) MES buffers. (c) The correlation between excitation wavelength and the peak of major emission band

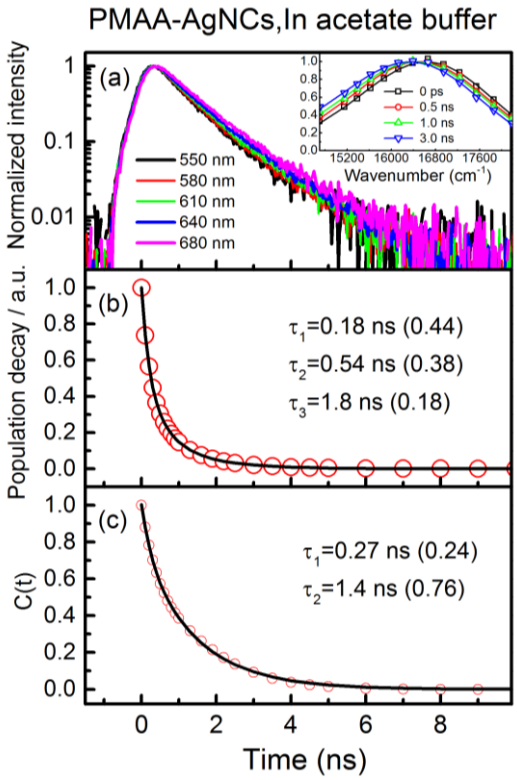

Figure 3: (a) The representative fluorescence transients and the reconstructed time-resolved emission spectra, (b) the population decay dynamics and (c) the spectral relaxation dynamics of the PMAA-AgNCs in acetate buffer.

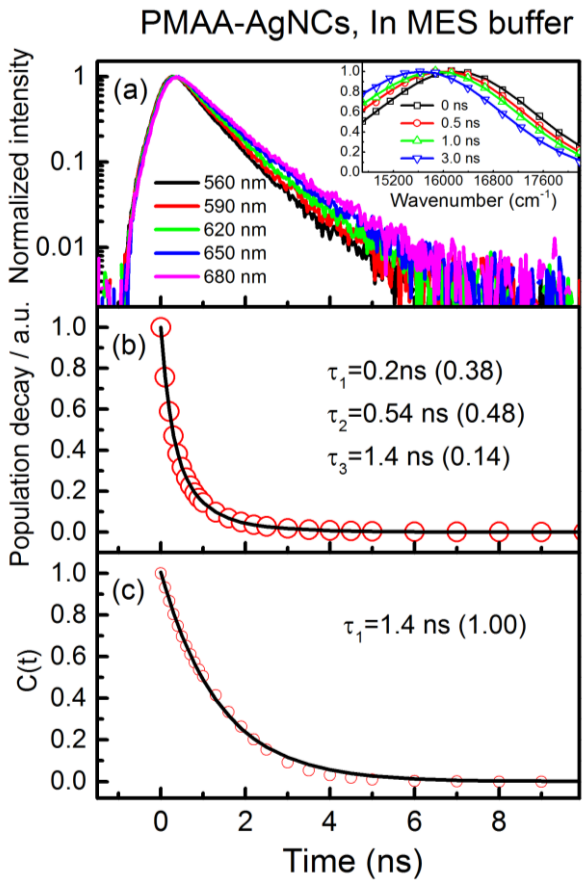

Figure 4: (a) The representative fluorescence transients and the reconstructed time-resolved emission spectra, (b) the population decay dynamics and (c) the spectral relaxation dynamics of the PMAA-AgNCs in MES buffer

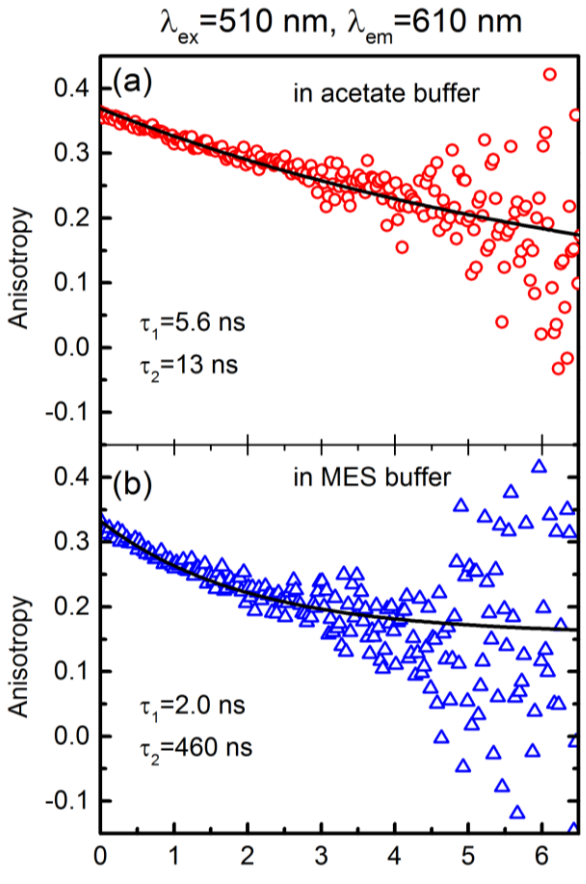

Figure 5: The fluorescence anisotropy decay dynamics of the PMAA-AgNCs in (a) acetate buffer (b) MES buffer. The solid curve indicates the bi-exponential fitting of the anisotropy decay dynamics.

suggests that the spectral relaxation is not due to the solvation processes. Another feasible mechanism that could cause the spectral relaxation is the energy transfer dynamics. This interpretation is supported by the increasing of relaxation energy upon 445 nm excitation ($\Delta\nu$=1421 cm^{-1} and 1776 cm^{-1} in the acetate and MES buffer, respectively; figure S_5 and S_6). According to these findings, the spectral relaxation dynamics of the PMAA-AgNCs are associated with the energy transfer dynamics and the excitation of the multiple emissive species that have different emission wavelengths and fluorescence lifetimes. The different emissive species are originated form the AgNCs that exhibits different interaction energy with the surrounding matrix. The larger spectral shift that we observed in the PVA film and solid powder reflects the higher structural heterogeneity of the PMAA-AgNCs in the solid matrix.

In this study, the fluorescence anisotropy decays of the PMAA-AgNCs are utilized to study the flexibility of the PMAA (figure 5). In the PVA film and solid powder, the anisotropy decays are time independent, which indicates that the motion of the polymer is inhibited in solid matrix (figure S_7). In the acetate and MES buffers, the anisotropy decay dynamics, r(t), are fitted by a bi-exponential model:

$$r(t) = a_1 e^{-t/\tau_S} + a_2 e^{-t/\tau_L} \quad (3)$$

where the τ_S and τ_L indicate the short and the long correlation time, respectively. The correlation time for the segmental motions (τ_{seg}) and the overall rotation of the macromolecule (τ_{rot}) can be represented by equation (4):[46]

$$\frac{1}{\tau_S} = \frac{1}{\tau_{seg}} + \frac{1}{\tau_{rot}}, \frac{1}{\tau_L} = \frac{1}{\tau_{rot}} \quad (4)$$

Because the fluorescence time window provided by the AgNCs is not long enough to determine the rotation time of the entire polymer, the τ_{rot} is fixed at the value obtained from the Perrin equation:

$$\tau_{rot} = \frac{V\eta}{RT} \quad (5)$$

In which η is the viscosity of water (0.89 mPa • s at 25°C), R is the gas constant, T is temperature (which is 298 K in our case) and V is the hydrodynamic volume ($V = \frac{4}{3}\pi r_H^3$, r_H= the hydrodynamic radius of PMAA) of the polymer. Based on the r_H obtained from the dynamic light scattering experiment (which is 2.4 nm in the acetate buffer and 8 nm in the MES buffer), the τ_{rot} of the PMAA in the acetate and MES buffers are fixed at the values of 13 ns and 460 ns, respectively. According to equation (4), the τ_{seg} of the PMAA-AgNCs decrease from 9.8 ns in the acetate buffer to 2.0 ns in the MES buffer. This finding suggests that the PMAA become more flexible in the MES buffer, which is consistent with the studies

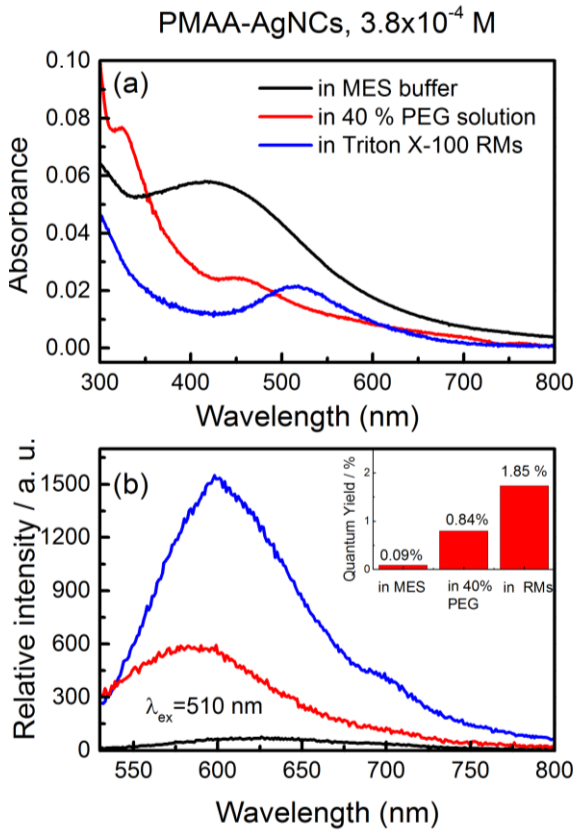

Figure 6: (a) The absorption and (b) emission spectra of the PMAA-AgNCs in dilute and molecular crowding conditions. The concentration indicates the strand concentration of the PMAA. The intensity of the emission spectra have been calibrated for the absorbance at excitation wavelength (divided by 1-10^{-A}; A is the absorbance at 510 nm). The inset shows the fluorescence quantum yields estimated by using the rhodamine 6G ethanol solution as reference.

using external chromophore.[36, 37] To evaluate the molecular crowding effect of the PMAA-AgNCs, the RMs and the 40 % (weight percentage) PEG 400 solution are employed to create the molecular crowding conditions.[40] The PMAA-AgNCs were encapsulated in the RMs made by three different surfactants: The AOT, CTAB and TritonX-100. The PMAA-AgNCs are prepared in the MES buffer and then added into the RMs.

Recent findings have demonstrated that the formation of emissive AgNCs requires both the neutral Ag^0 atoms and positively charged Ag^+ cations.[47] Therefore, the presence of anionic head groups in the AOT RMs and the Br^- ions in the CTAB RMs are deleterious for the fluorescence of PMAA-AgNCs,[48] and the fluorescence of the PMAA-AgNCs is completely diminished in these two RMs (Figure S_8). Figure 6 represents the absorption and emission spectra of the PMAA-AgNCs in the MES buffer, 40 % PEG 400 solution and Triton X-100 RMs. In the 40 % PEG 400 solution and Triton X-100 RMs, the fluorescence quantum yields of the PMAA-AgNCs are estimated to be 0.84 % and 1.85 %, respectively. By measuring the fluorescence quantum yield of the PMAA-AgNCs in different percentages of glycerol solutions, we find that the fluorescence quantum yield of the PMAA-AgNCs display a good correlation with the viscosity of solvent (Figure 7). The result implies that the PMAA-AgNCs can be used as the viscosity probe. The microviscosity in the 40 % PEG 400 solution and Triton-X 100 RMs water pool are thus estimated to be about

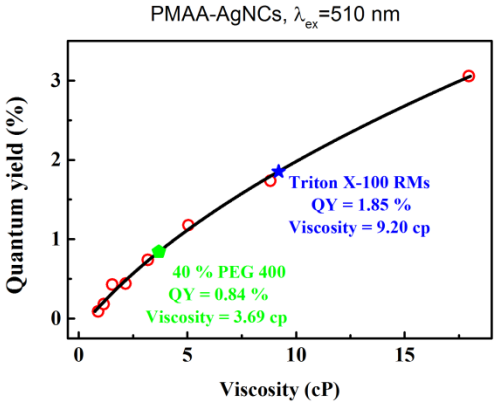

Figure 7: The fluorescence quantum yields of PMAA-AgNCs in different percentages of glycerol solutions (the red circle), 40 % PEG 400 solution (the green pentagon) and the Triton X-100 RMs (the blue star).

3.7 cP and 9.2 cP, respectively. The viscosity obtained in the 40 % PEG 400 solution is consistent with the value obtained from commercial Ubbelohde type viscometer.[49] Meanwhile, the PMAA-AgNCs also reveal spectral relaxation in the 40% PEG 400 solution (Figure S_9) and the Triton-X 100 RMs (Figure S_{10}). The C(t) in the molecular crowding condition closely resembles that in the dilute solution. Our finding suggested that the spectral relaxation of the PMAA-AgNCs is not due to the solvation process, and it is associated with the energy transfer dynamics and the excitation and multiple emissive AgNCs.

Conclusions

In this study, the fluorescence properties of the silver nanocluster synthesized in the polymer template are investigated using steady state and time-resolved fluorescence spectroscopy. In the acetate buffer, the emission peak of the PMAA-AgNCs is located at $\lambda_{excitation}/\lambda_{emission}$=490 nm/580 nm, and the fluorescence quantum yield is estimated to be 1.14 %. In the MES buffer, fluorescence quantum yield substantially decreased to 0.09 % and the emission peak bathochromic shifted to $\lambda_{excitation}/\lambda_{emission}$=505 nm/610 nm. The lower fluorescence quantum yield of the PMAA-AgNCs in the MES buffer is associated with the fluorescence quenching caused by the hydrogen bond between the AgNCs and solvent.[50, 51] Meanwhile, we have performed complete analysis on the time-resolved emission spectra of the PMAA-AgNCs. Our study confirms that the spectral relaxation dynamics of the PMAA-AgNCs are originated from the energy transfer dynamics and the excitation of the multiple emissive species that exhibit different interaction energy with the surrounded matrix. The PMAA-AgNCs is also employed as the fluorescence probe for study the anisotropy dynamics in different PMAA conformations. The results reflect the higher backbone flexibilities of the PMAA in the water swollen conformation, which is in good agreement with the study using external chromophore. In this study, we reported the feasibly of using the PMAA-AgNCs as the viscosity probe for studying the microviscosity of the environment. In the molecular crowding conditions created by 40 % PEG 400 solution and Triton X-100

RMs, the viscosity was estimated to be 3.7 and 9.2 cP, respectively.

In summary, we have demonstrated the feasibility of using the AgNCs as the fluorescence probe for studying the environment heterogeneity and the backbone flexibility of the polymer. Those results are important applying the AgNCs in studying the conformation and the local environment of the template. The molecular crowding studies confirm that the PMAA-AgNCs represents higher fluorescence quantum yields in the molecular crowding conditions, which is beneficial for their usage in the intracellular environments. To our knowledge, this is the first molecular crowding study on the PMAA-AgNCs, and the information that we provide is crucial for their future applications in biological studies.

Acknowledgements

We sincerely appreciate the support from the Ministry of Science and Technology, Taiwan, ROC (Project contracts: NSC 102-2113-M-018-005-MY2). We also thank Ms. Sophie Yun-Chen Wu for her modification in this manuscript

References

1 J. M. Obliosca, C. Liu and H.-C. Yeh, *Nanoscale*, 2013, **5**, 8443-8461.
2 I. Díez and R. H. A. Ras, *nanoscale*, 2011, **3**, 1963-1970.
3 C.-A. J. Lin, C.-H. Lee, J.-T. Hsieh, H.-H. Wang, J. K. Li, J.-L. Shen, W.-H. Chan, H.-I. Yeh and W. H. Chang, *J. Med. Biol. Eng.*, 2009, **29**, 276-283.
4 S. W. Yang and T. Vosch, *Anal. Chem.*, 2011, **83**, 6935-6939.
5 W. Guo, J. Yuan, Q. Dong and E. Wang, *J. Am. Chem. Soc.*, 2009, **132**, 932-934.
6 H.-C. Yeh, J. Sharma, J. J. Han, J. S. Martinez and J. H. Werner, *Nano Lett.*, 2010, **10**, 3106-3110.
7 I. Díez, M. Pusa, S. Kulmala, H. Jiang, A. Walther, A. S. Goldmann, A. H. E. Müller, O. Ikkala and R. H. A. Ras, *Angew. Chem. Int. Ed.* , 2009, **48**, 2122-2125.
8 C. I. Richards, S. Choi, J.-C. Hsiang, Y. Antoku, T. Vosch, A. Bongiorno, Y.-L. Tzeng and R. M. Dickson, *J. Am. Chem. Soc.*, 2008, **130**, 5038-5039.
9 L. Shang and S. Dong, *Chem. Commun*, 2008, 1088-1090.
10 B. Sengupta, C. M. Ritchie, J. G. Buckman, K. R. Johnsen, P. M. Goodwin and J. T. Petty, *J. Phys. Chem. C*, 2008, **112**, 18776-18782.
11 T. Vosch, Y. Antoku, J.-C. Hsiang, C. I. Richards, J. I. Gonzalez and R. M. Dickson, *Proc. Natl. Acad. Sci. U.S.A.*, 2007, **104**, 12616-12621.
12 J. Zhang, S. Xu and E. Kumacheva, *Adv. Mater*, 2005, **17**, 2336-2340.
13 J. T. Petty, J. Zheng, N. V. Hud and R. M. Dickson, *J. Am. Chem. Soc.*, 2004, **126**, 5207-5212.
14 J. Zheng and R. M. Dickson, *J. Am. Chem. Soc.* , 2002, **124**, 13982-13983.
15 S. Choi, R. M. Dickson and J. Yu, *Chem. Soc. Rev.*, 2012, **41**, 1867-1891.
16 Z. Huang, Y. Tao, F. Pu, J. Ren and X. Qu, *Chem. Eur. J.*, 2012, **18**, 6663-6669.
17 J. Zheng, P. R. Nicovich and R. M. Dickson, *Annu. Rev. Phys. Chem.*, 2007, **58**, 409-431.
18 G. Schmid, *Chem. Rev.*, 1992, **92**, 1709-1727.
19 K. Ryogo, *J. Phys. Soc. Jpn*, 1962, **17**, 975.
20 I. Díez and R. H. A. Ras, *Few-atom silver clusters as fluorescent reporters*, Speringer-Verlag 2010.
21 Z. Yuan, N. Cai, Y. Du, Y. He and E. S. Yeung, *Anal. Chem.*, 2013, **86**, 419-426.
22 L. Shang and S. Dong, *J. Mater. Chem.* , 2008, **18**, 4636-4640.
23 L. Shang and S. Dong, *Chem. Commun.*, 2008, 1088-1090.
24 X. Yuan, Z. Luo, Q. Zhang, X. Zhang, Y. Zheng, J. Y. Lee and J. Xie, *ACS Nano*, 2011, **5**, 8800-8808.
25 C. M. Ritchie, K. R. Johnsen, J. R. Kiser, Y. Antoku, R. M. Dickson and J. T. Petty, *J. Phys. Chem. C*, 2007, **111**, 175-181.
26 B. Sengupta, K. Springer, J. G. Buckman, S. P. Story, O. H. Abe, Z. W. Hasan, Z. D. Prudowsky, S. E. Rudisill, N. N. Degtyareva and J. T. Petty, *J. Phys. Chem. C*, 2009, **113**, 19518-19524.
27 J. T. Petty, C. Fan, S. P. Story, B. Sengupta, A. S. J. Lyer, Z. Prudowsky and R. M. Dickson, *J. Phys. Chem. Lett*, 2010, **1**, 2524-2529.
28 L. Feng, Z. Huang, J. Ren and X. Qu, *Nucleic acids res.*, 2012, **40**, e122.
29 Y. Tao, Z. Li, E. Ju, J. Ren and X. Qu, *Chem. Commun.*, 2013, **49**, 6918-6920.
30 Y. Tao, Y. Lin, Z. Huang, J. Ren and X. Qu, *Talanta*, 2012, **88**, 290-294.
31 Z. Zhou, Y. Du and S. Dong, *Biosens. Bioelectron.* , 2011, **28**, 33-37.
32 J. Sharma, H.-C. Yeh, H. Yoo, J. H. Werner and J. S. Martinez, *Chem. Commun*, 2011, **47**, 2294-2296.
33 J. Yu, S. Choi and R. M. Dickson, *Angew. Chem. Int. Ed.*, 2009, **48**, 318-320.
34 F. Qu, L. L. Dou, N. B. Li and H. Q. Luo, *J. Mater. Chem. C*, 2013, **1**, 4008-4013.
35 H.-C. Hsu, M.-C. Ho, K.-H. Wang, Y.-F. Hsu and C.-W. Chang, *New. J. Chem.*, 2015, **39**, 2140-2145.
36 L. Ruiz-Pérez, A. Pryke, M. Sommer, G. Battaglia, I. Soutar, L. Swanson and M. Geoghegan, *Macromolecules*, 2008, **41**, 2203-2211.
37 I. Soutar and L. Swanson, *Macromolecules*, 1994, **27**, 4304-4311.
38 M. K. Kuimova, G. Yahioglu, J. A. Levitt and K. Suhling, *J. Am. Chem. Soc.*, 2008, **130**, 6672-6673.
39 A. P. Minton, *J. Biol. Chem.*, 2001, **276**, 10577-10580.
40 D. Miyoshi and N. Sugimoto, *Biochimie*, 2008, **90**, 1040-1051.
41 W. D. V. Horn, M. E. Ogilvie and P. F. Flynn, *J. Am. Chem. Soc.*, 2009, **131**, 8030-8039.
42 M.-C. Ho and C.-W. Chang, *RSC advances*, 2014, **4**, 20531-20534.
43 Y. Chen, T. Yang, H. Pan, Y. Yuan, L. Chen, M. Liu, K. Zhang, S. Zhang, P. Wu and J. H. Xu, *J. Am. Chem. Soc.*, 2014, **136**, 1686-1689.
44 I. Díez, R. H. A. Ras, M. I. Kanyuk and A. P. Demchenko, *Phys. Chem. Chem. Phys.*, 2013, **15**, 979-985.
45 M. L. Horng, J. A. Gardecki, A. Papazyan and M. Maroncelli, *J. Phys. Chem.*, 1995, **99**, 17311-17337.
46 J. R. Lakowicz, *Principle of fluorescence spectrosocpy*, Springer, 2006.
47 D. Schultz, K. Gardner, S. S. R. Oemrawsingh, N. Marksševic, K. Olsson, M. Debord, D. Bouwmeester and E. Gwinn, *Adv. Mater.*, 2013, **25**, 2797-2803.
48 J. Peng, Y. Shao, L. Liu, L. Zhang, W. Fu and H. Liu, *Nanotechnology*, 2014, **25**.
49 F. Han, J. Zhang, G. Chen and X. Wei, *J. Chem. Eng. Data*, 2008, **53**, 2598-2601.
50 T. Udaya, B. Rao and T. Pradeep, *Angew. Chem. Int. Ed.*, 2010, **49**, 3925-3929.
51 Y. Li, X. Wang, S. Xu and W. Xu, *Phys. Chem. Chem. Phys.*, 2013, **15**, 2665-2668.